Available online at www.sciencedirect.com
SCIENCE DIRECT
ELSEVIER
Palaeogeography, Palaeoclimatology, Palaeoecology 236 (2006) 135–150
PALAEO
www.elsevier.com/locate/palaeo

Modelling iceberg trajectories, sedimentation rates and meltwater input to the ocean from the Eurasian Ice Sheet at the Last Glacial Maximum

Ros Death [a,*], Martin J. Siegert [a], Grant R. Bigg [b], Martin R. Wadley [c]

[a] *Bristol Glaciology Centre, School of Geographical Sciences, University of Bristol, University Road, Bristol, BS8 1SS, UK*
[b] *Department of Geography, University of Sheffield, Sheffield, UK*
[c] *School of Environmental Sciences, University of East Anglia, Norwich, NR4 7TJ, UK*

Received 30 September 2004; accepted 11 November 2005

Abstract

We model iceberg flow paths from the Eurasian Ice Sheet, and the associated meltwater production and sedimentation rates within the Norwegian–Greenland Sea during the last glaciation. Results from a numerical ice sheet model, an atmospheric general circulation model and an ocean general circulation model are collated and used to provide iceberg production rate, wind field and surface current forcings to an iceberg trajectory model. The iceberg model then determines how icebergs issuing from the Eurasian Ice Sheet travel across the ocean and eventually melt. In addition the release of iceberg sediments is also predicted. The results show that iceberg trajectories are complex and that common features of iceberg movement are clustering in zones of convergence and exit into the North Atlantic through the Iceland–Faeroes Channel. Eurasian icebergs do not penetrate into the interior of the Arctic Ocean. The gathering of icebergs produces a complex meltwater pattern that does not follow the conceptual idea of decreasing meltwater production with distance from the ice sheet margin. Sedimentation results are compared with the meltwater configuration and are found to be a poor indicator of past zones of iceberg melt, with zones of sedimentation extending significantly less far.
© 2006 Elsevier B.V. All rights reserved.

Keywords: Icebergs; Ice sheet; Ice Rafted Debris; Meltwater; Greenlad–Iceland–Norwegian Seas; Late Quaternary

1. Introduction

Modelling iceberg discharge from ice sheets is critical to evaluating their role in perturbing the state of the oceans during glacial periods. Meltwater pulses within the North Atlantic, as identified by excursions in $\delta^{18}O$ within marine sediment records (Bard et al., 2000), are associated with the presence of Ice Rafted Debris (IRD), thereby implicating the role of icebergs in salinity changes (Heinrich, 1988; Bond et al., 1993; Grousset et al., 1993; Dowdeswell et al., 1995; Grousset et al., 2001).While attention has been paid to modelling the decay of the Laurentide ice sheet (MacAyeal, 1993; Alley, 1998), little focus has yet been placed on quantifying the glacial products of the Eurasian Ice Sheet in the Late Quaternary. Such information is critical to reconstructing the supply of freshwater to the Greenland–Iceland–Norwegian (GIN) Seas, the North Atlantic and the Arctic Ocean.

* Corresponding author.
E-mail address: ros.death@bristol.ac.uk (R. Death).

0031-0182/$ - see front matter © 2006 Elsevier B.V. All rights reserved.
doi:10.1016/j.palaeo.2005.11.040

At the Last Glacial Maximum (LGM) an ice sheet occupied Scandinavia, extending northwards into the Barents Sea, and parts of the Kara Sea, and stretching south to cover the northern region of the British Isles. The boundaries of the ice sheet are well defined through both numerical modelling and geological data sets (Svendsen et al., 1999). In particular two projects, Polar North Atlantic Margins (PONAM), from 1990–1995, and the subsequent program Quaternary Environments of the Eurasian North (QUEEN), from 1996–2002, specifically aimed to increase the level of glacial-geologic data in this region. The resulting ice sheet limits at the LGM are fully described by Svendsen et al. (1999) and illustrated in Fig. 1. The western margin and parts of the northern margin are well defined by sequences of marine sediments on the adjacent continental shelf edge, indicating that the ice sheet reached the shelf break. Furthermore, the marine sequences also locate where major ice streams were active through glacial cycles, through the presence of large trough mouth fans. Of particular interest to this study is that both the western and northern margins of the ice sheet are marine based and therefore, loss of ice would have most likely occurred through iceberg calving (Siegert et al., 2002).

The discharge of ice into the GIN Seas is of great interest, as in the present day these seas are one of the sources of deep water production and, therefore, changes in this region can be transmitted globally. Additionally, these seas are oceanographically sensitive to changes in salinity and temperature, and thereby meltwater from the Eurasian and Greenland ice sheets. Evidence that the LGM circulation was indeed different is provided through a number of palaeoclimate and palaeoceanographic indicators (Koç et al., 1993; Hebbeln et al., 1998; Bauch et al., 2001). The most documented difference is North Atlantic Deep Water (NADW) production being further south than the Norwegian Seas and weakened, so it formed

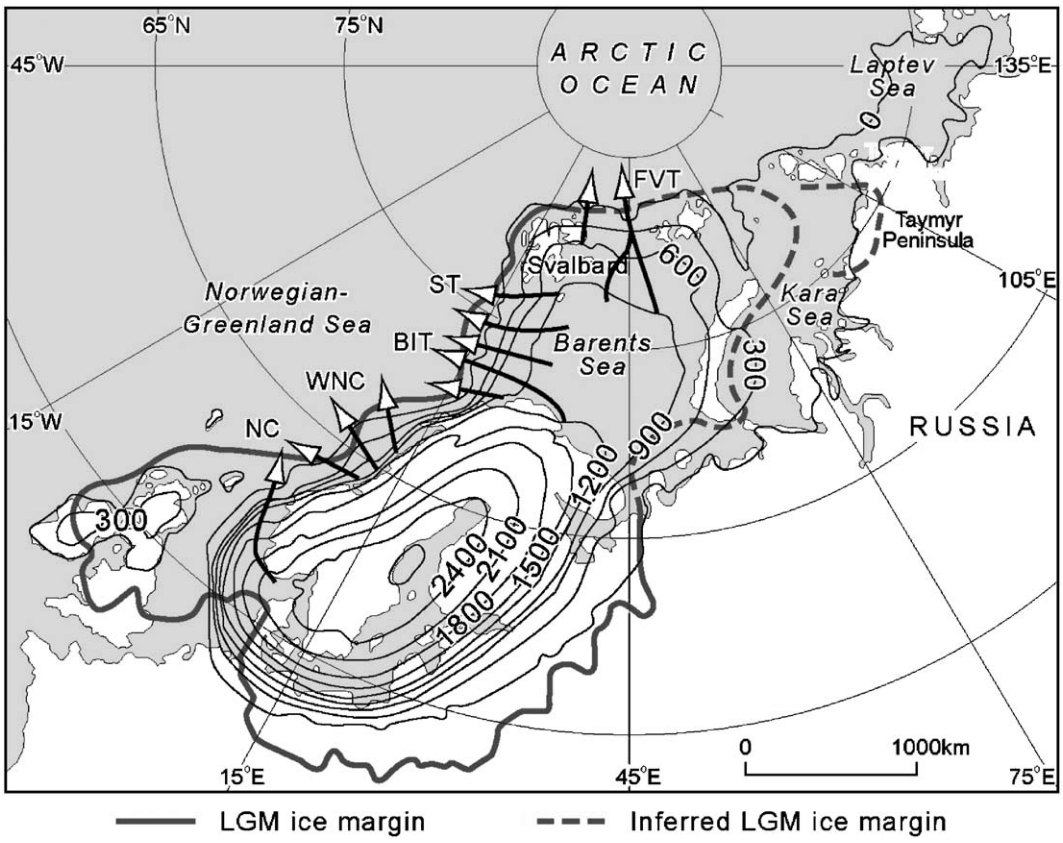

Fig. 1. The Eurasian Ice Sheet thickness at the LGM as modelled by Siegert et al. (1999). Contours are provided every 300 m. The flow directions and locations of major ice streams within the Norwegian Channel (NC), a series of western Norwegian Channels (WNC), the Bear Island Trough (BIT), Storfjorden (ST) and the Franz Victoria Trough (FVT) are denoted by arrows. Also shown is the ice sheet margin derived from geological evidence as a thick grey line (after Svendsen et al., 1999).

waters that occupied more intermediate depths (Sarnthein et al., 1995; Duplessy et al., 2002; Rahmstorf, 2002). An indicator of this weakened NADW export is the decrease in the gradient between Pacific and Atlantic $\delta^{13}C$ concentrations (Raymo et al., 1990). Further evidence for a reduction in NADW strength is the decrease in the average silt size, a proxy for bottom-current strength, where the present day Iceland–Scotland overflow water and Denmark Strait water are located (Prins et al., 2002).

In coupled atmosphere–ocean modelling of the LGM the correct spatial and temporal distribution of meltwater input, and its magnitude, is required in order to reproduce ocean conditions accurately. Although currently it might be assumed that meltwater input will decrease with distance from the ice margin, if the meltwater input is from icebergs the pattern may be more complex. The aim of this paper is to provide a characterisation of how icebergs released by the Eurasian Ice Sheet at the LGM supplied meltwater and sediment to the GIN Seas and the North Atlantic.

2. Modelling iceberg trajectories

This investigation uses an iceberg trajectory model to describe the flow of icebergs across an ocean. Clarke and La Prairie (2001) distinguish two distinct approaches to evaluating the freshwater release from icebergs, the 'Titanic' and the 'Heinrich' procedures. The 'Titanic' method is based on the individual tracks of the iceberg (Matsumoto, 1996, 1997), whereas the 'Heinrich' method is a distributed approach, which concentrates more on the freshwater envelope created by the melting of a group of icebergs (Clarke and La Prairie, 2001). The methodology behind the iceberg model used here follows the 'Titanic' approach, in that the path of each iceberg released is determined, based on the physics controlling the iceberg's motion and the evolution of its shape and size. Iceberg calving results from a numerical ice sheet model are used as input to the iceberg model. Ocean and atmospheric general circulation model results are used as forcing conditions in the iceberg model. Details of the model, and input data, are given below.

2.1. Iceberg model

An iceberg trajectory model, developed and described by Bigg et al. (1997), is used to determine the drift and deposition of icebergs seeded from the Eurasian Ice Sheet at the LGM. The iceberg model has both a dynamic and thermodynamic component. The dynamic component is described by:

$$M\frac{\partial V_i}{\partial t} = -MfV_i + F_p + F_w + F_r + F_a + F_s \quad (1)$$

where M is the mass of the iceberg, V_i is the iceberg velocity, f is the Coriolis parameter, F_p is the pressure gradient force, F_r is the wave radiation force, and the remaining terms are the drag terms; F_w, the water drag, F_a, the air drag and F_s, the sea–ice drag.

To a large extent, the horizontal velocity of the iceberg is determined by the ocean current within which it is advected. The iceberg model assumes that the iceberg's long axis is parallel to the current and therefore the wind stress is acting at 45° to the left of the iceberg (for the northern hemisphere), in agreement with Ekman theory. Once the iceberg is in motion a number of additional terms act on the iceberg. In the northern hemisphere the Coriolis force acts to deflect the icebergs to the right. Additionally a number of frictional drag terms also are generated, for which the general drag equation is:

$$F_x = \frac{1}{2}\rho_x C_x A_x |V_x - V_i|(V_x - V_i) \quad (2)$$

where ρ_x is the density, C_x is the drag coefficient, A_x, represents the appropriate cross-sectional area of the iceberg in contact with the drag-producing medium, V_x is the velocity of the drag-producing medium and V_i is the velocity of the iceberg. The subscript x is interchanged for air, water and sea–ice.

The thermodynamic component of the model is important as it controls the mass and shape of the iceberg through time, and thereby the way in which the dynamic forces act on the iceberg which determines its trajectory. The model takes into account; turbulent heat transfer, buoyant convection, wave erosion and, for completeness, sensible heating and sublimation at the ice–air interface (Bigg et al., 1997; Gladstone et al., 2001). The latter two components are much smaller than the melting and wave erosion that occurs at the ice–water interface. Iceberg mass is able to increase with the addition of solid precipitation, which can occur if the air temperature is less than 0 °C. A complete description of the model's thermodynamic component is provided by Bigg et al. (1997).

2.2. Iceberg inputs

Results from a numerical ice sheet model (Siegert et al., 1999) are used to supply the iceberg model with positions and rates of iceberg releases from the Eurasian

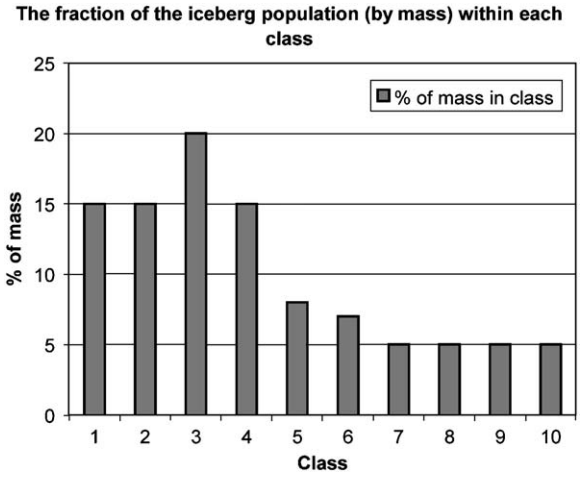

Fig. 2. The log-normal distribution of decreasing numbers of icebergs with increasing size, with the majority of icebergs having a length less than 500 m (class 5 and smaller), in agreement with observations from Weeks and Mellor (1978) and Dowdeswell et al. (1992).

Ice Sheet at the LGM (Fig. 1). As the ice sheet and iceberg models run over different topographic projections (the ice sheet model uses a fixed 20×20 km grid, whereas the iceberg model runs over a rotated 1° latitude/longitude domain), the ice sheet model results were geo-rectified onto the iceberg model's grid. Icebergs were released at 20 km intervals along the ice sheet's marine margin (as in the ice sheet model). The flux of ice released was converted into a mass, and this was distributed between 10 classes of icebergs as proposed by Bigg et al. (1997), based on observations of icebergs in the Arctic at the present day (Dowdeswell et al., 1992) (Fig. 2). The general trend between number of icebergs released and iceberg length is a lognormal distribution (Bigg et al., 1997). Determination of the iceberg's other dimensions is described fully in Bigg et al. (1997), based on observations of icebergs in the northern hemisphere. The dimensions of the resulting ten iceberg classes are summarised in Table 1. It should be noted that this class division, while including the total mass output from the ice sheet, ignores production of giant, multi-kilometre sized, icebergs, as likely occurred from the marine-based part of the Eurasian Ice Sheet, and as does occur from today's Antarctica. However, as the iceberg model replicates observed iceberg limits in the Antarctic (Gladstone et al., 2001) this is not thought to be a significant limitation of our analysis.

2.3. Model boundary conditions and forcing fields

The bathymetry used by the iceberg model is derived from the DBDB5 data set and is used to determine if an iceberg keel is greater than the water depth it occupies, in which case it becomes grounded until it melts enough to refloat. The iceberg model uses a land mask to delineate between ocean and land. The model topography used in this study is a combination of the original iceberg model topography, which for the glacial topography uses the Peltier 21–0 ka adjustment added to the present day topography from the NGDC (1986) 5×5 data set, and the ice sheet model elevations from Siegert et al. (1999). The final topography for the LGM is shown in Fig. 3. If an iceberg collides with the coast it is assumed to melt out at that point. This might bias melt close to the coast as icebergs are observed to refloat after a period of being stranded, however analysis of model results presented here suggests this problem is minor (Gustajitis and Buckley, 1978; Bigg et al., 1997).

The iceberg model requires a number of oceanic and atmospheric forcing fields to drive the dynamic and thermodynamic routines. To capture seasonal variation monthly data are provided for the seven forcing fields used; sea-surface temperature (°C), meridional surface ocean current (cm s^{-1}), zonal surface ocean current (cm s^{-1}), meridional surface wind stress (dynes cm^{-2}), zonal wind stress (dynes cm^{-2}), air temperature (°C), precipitation (mm). The atmospheric forcing fields of air temperature, precipitation, and wind stress are provided from the simulation by Dong and Valdes (1998) of the LGM using the Universities Global Atmospheric Modelling Programme (UGAMP) General Circulation Model (GCM). These atmospheric forcing fields, with an additional freshwater flux of 1 mm day^{-1} in the North Atlantic region of 60–75°N, are used to force an Ocean General Circulation Model, which is based on the Southampton–East Anglia (SEA) model that produces the sea-surface temperature, and ocean currents (Wadley et al., 2002).

Table 1
The percentage of total mass flux through a cell assigned to each class and the dimensions of each class

Size class	Fraction of population by mass (%)	Length (m)	Width (m)	Draught (m)	Freeboard (m)	Mass (10^9 kg)
1	15	100	67	67	13.4	0.491
2	15	200	133	133	26.5	3.88
3	20	300	200	200	40.0	13.1
4	15	400	267	267	53.0	31.2
5	8	500	333	300	60.0	54.7
6	7	600	400	300	60.0	78.8
7	5	750	500	300	60.0	123.0
8	5	900	600	300	60.0	177.0
9	5	1200	800	300	60.0	315.0
10	5	1500	1000	300	60.0	492.0

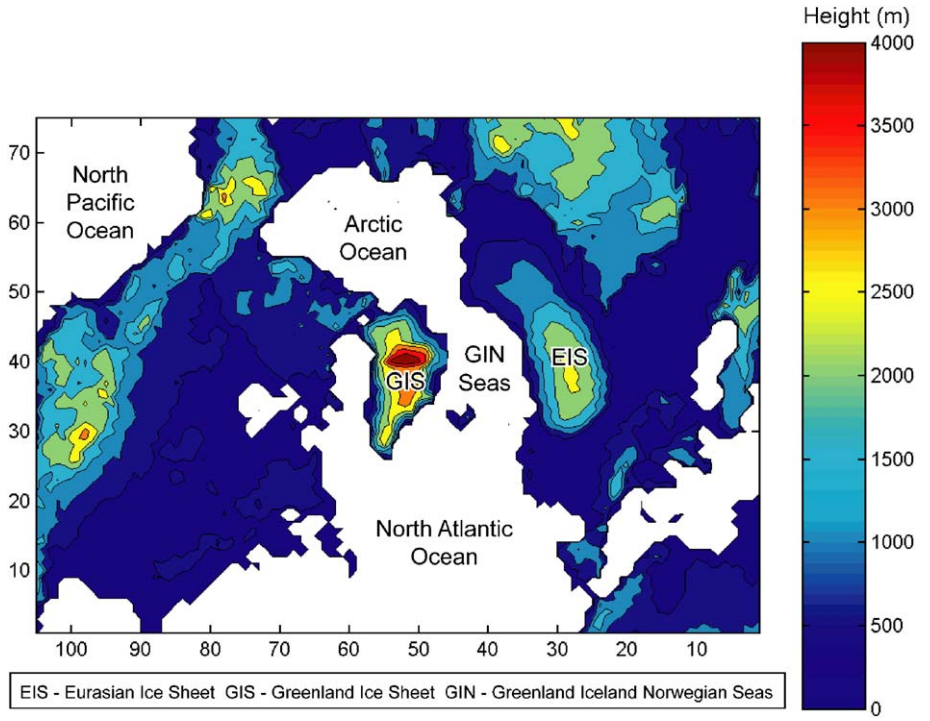

Fig. 3. The combined topography of the original iceberg model's glacial topography and the addition of the Eurasian Ice Sheet topography as determined by Siegert et al. (1999), shown in the model grid projection.

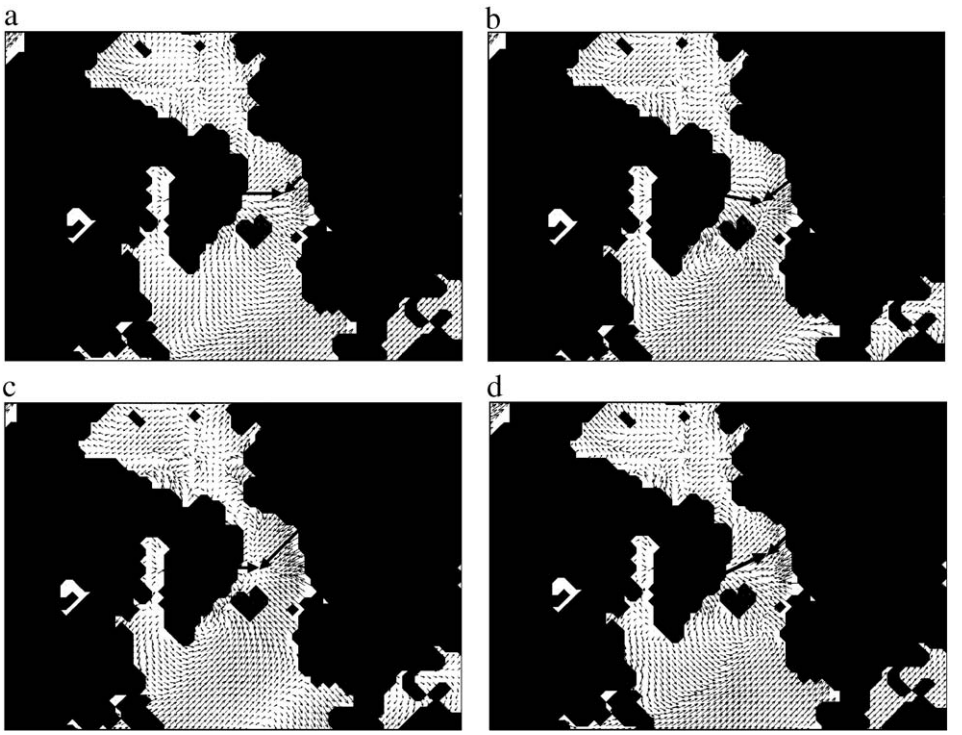

Fig. 4. Glacial surface wind stress (generated using for the Greenland–Norwegian–Iceland region, for the four seasonal months, March (a), June (b), September (c), and December (d) (shown in the model grid projection). The heavy black arrows illustrate the dominant wind path off the Norwegian and Greenland coasts. Atmospheric fields used in the model are generated with the UGAMP GCM.

In any attempt to recreate or predict iceberg trajectory and melt, an accurate understanding of the data that are used in the model is paramount for the correct interpretation of the results. Therefore, the three most dominant forcing fields for computing an iceberg's dynamic and thermodynamics, which are the wind stress, the ocean current and the sea-surface temperature, will be described.

The seasonal variation in wind stress is illustrated in Fig. 4a–d. The most notable feature in the wind stress fields is the strong winds off both the Norwegian and Greenland coast (see heavy black arrows) that results in the convergence zone in the Norwegian–Greenland Sea. Throughout the year the direction and strength of these winds vary resulting in the movement of the convergence zone back and forth across the Norwegian–Greenland basin. In June the wind stress in this region has a more southward component, while in September the Greenland wind component weakens relative to the Norwegian wind causing the convergence zone to shift towards the Greenland coast. In the winter months the wind off Greenland increases again and the convergence zone shifts back towards the Norwegian coast.

The ocean currents' seasonal variation is more difficult to capture schematically (Fig. 5). The general ocean model state at the LGM is a weakened North Atlantic Current, which in turn has a weaker branch of the Norwegian current. The Norwegian current travels up the Norwegian coast before turning westwards, and then southwards where the main wind convergence zone occurs in the centre of the Norwegian–Greenland basin. Additionally, the glacial model of the sub-polar gyre is of interest to this study (circled in grey). This differs from the present day sub-polar gyre by shifting further south. In general, the summer months (June and September) have a weaker overall circulation, which strengthens in the winter months (December). The surface wind stress is important in forcing the surface ocean, so the relative change in strength of the wind issuing from the Greenland and Norwegian land masses causes slight changes in the strength of westward current from the Norwegian coast: 5 cm s^{-1} in August, compared to 7 cm s^{-1} in January. The change is not as pronounced as seen in the wind stress as the ocean is not entirely wind-driven and so is unable to respond fast enough to capture the seasonal variation completely.

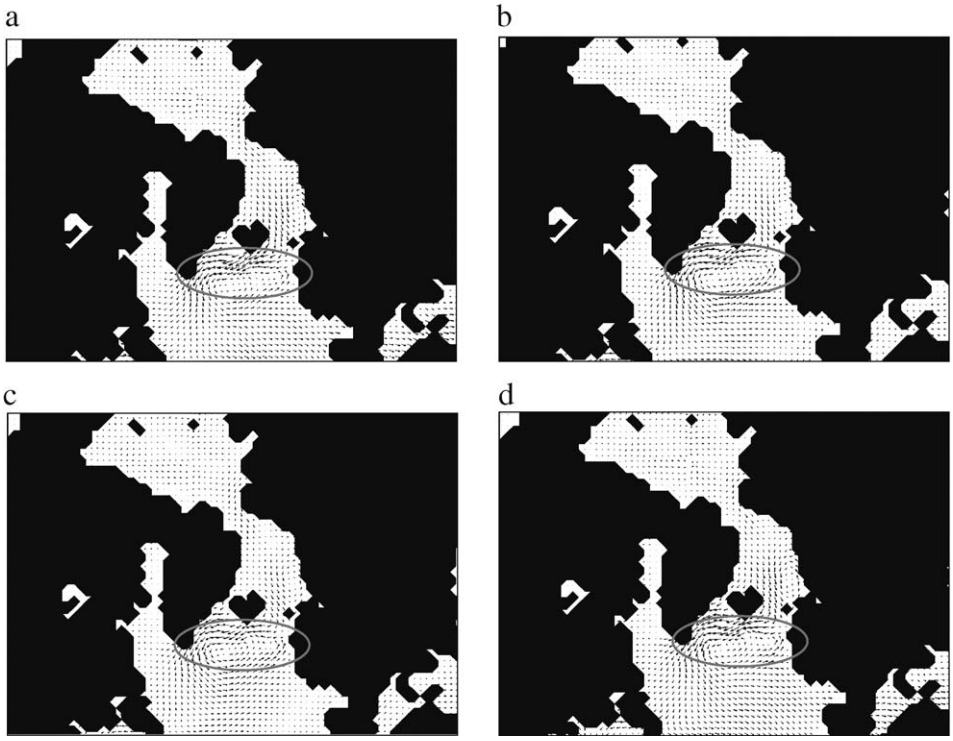

Fig. 5. Glacial ocean surface currents for the Greenland–Norwegian–Iceland Seas, for the four seasonal months, March (a), June (b), September (c), and December (d) (shown in the model grid projection). The sub-polar gyre is circled in grey. Ocean fields in the model are generated with an OGCM based on the SEA model.

Finally, the sea-surface temperature (SST) is shown for the same seasonal periods. The SSTs in the glacial model are below zero for most of the year in the Norwegian–Greenland basin, with a tongue of warmer water, 2 to 4 °C, being carried northwards by the North Atlantic Current which then follows the glacial sub-polar gyre, kinking westwards. The SST minima in this region is in the spring (March), and the warming in the summer occurs firstly along the Norwegian coast (June), before spreading across the basin towards Greenland (September). The modelled glacial SST maxima occurs in September, with water temperatures reaching just above zero, 0–1 °C, in the southern parts of the Norwegian–Greenland basin, before the temperatures begin cooling again towards winter (December). The rate at which SSTs increase in this region is much slower that the rate at which they decrease, illustrated by the asymmetry in the cycle of warming and cooling in Fig. 6a–d.

2.4. Modelling strategy and numerical procedure

Icebergs were released at 20 km intervals along the ice sheet margins in the Norwegian and Barents Sea for each month, January to December, and for each class, one to ten. In so doing the sensitivity of the iceberg size and forcing conditions to the icebergs trajectories and melt rates was evaluated. Each model run was for five years which allowed all icebergs, apart from those in the Arctic Ocean, to melt. At each time-step the model interpolates the forcing fields to the position of each individual iceberg, and solves a simple discretisation of Eq. (1) to calculate each iceberg's horizontal velocity. In addition, at each time step the iceberg model works out the various melt terms and recalculates the iceberg's new mass and dimensions.

The model results were recorded every half day, and provided a continuous log of each iceberg's position, velocity and dimensions, from which the iceberg's track, meltwater production and sedimentation rate were calculated. The meltwater production was calculated by summing up all the mass lost from icebergs within each grid cell over the entire model run. The meltwater production is summarised into small (class 1 to class 3), medium (class 4 to class 7) and large (class 8 to class 10) icebergs for each start month. The sedimentation rates were calculated by implementing a procedure based on the observations by Dowdeswell and Murray (1990),

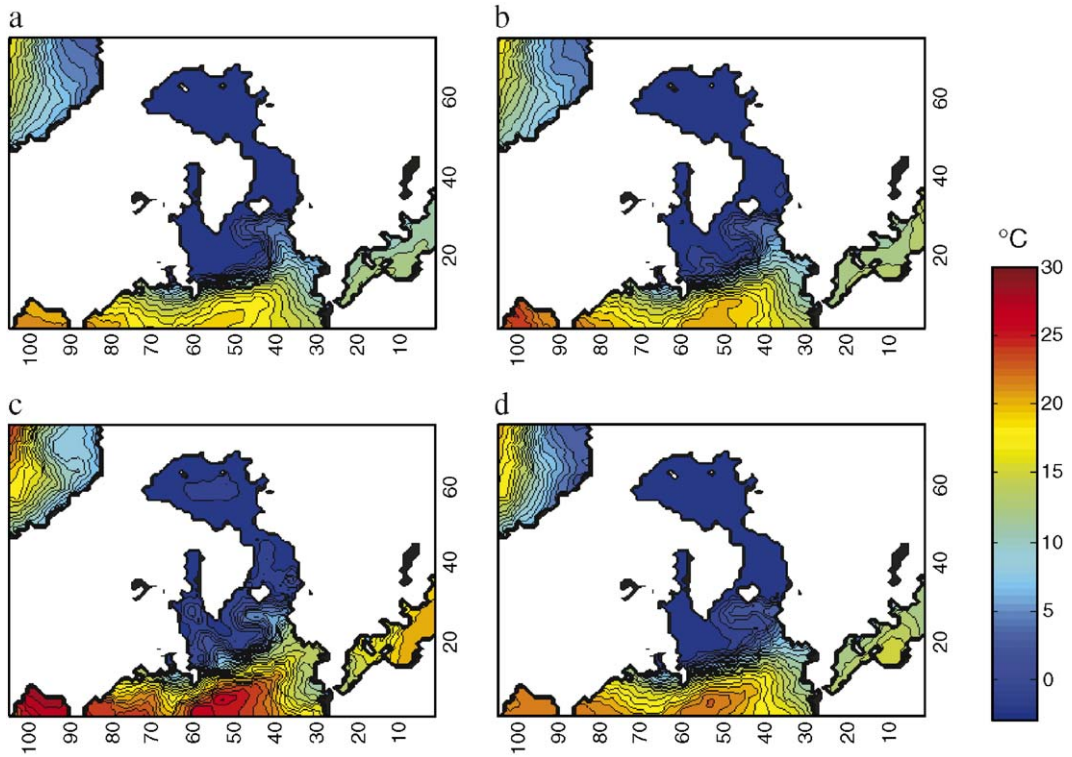

Fig. 6. Glacial sea-surface temperatures for the Greenland–Norwegian–Iceland Seas, for the four seasonal months, March (a), June (b), September (c), and December (d). Same model as for Fig. 5 (shown in the model grid projection).

and their conceptual model of sediment distribution through an iceberg. The model used in this study assumes sediment is carried in the bottom 10% of the iceberg and distributed between three layers. The first layer assumes that the sediment concentration is 10%, the second layer 5%, with 1% in the third layer. A routine was implemented to keep track of the basal melt loss from each iceberg at each time-step. As with meltwater production, the sedimentation rates were summed for each grid cell for small, medium and large classes of icebergs for each of the start months.

3. Model results

Iceberg trajectories are shown for the four seasonal months (March, June, September, and December) to illustrate the seasonal variation in forcing fields. The results are shown firstly for iceberg classes 1–5, and then for iceberg classes 5–10, in order that the diagrams do not become too confusing. Meltwater production and sedimentation rates are for all classes of icebergs that were seeded in the particular month being considered.

3.1. Iceberg tracks

Figs. 7–9 and 10a and b show the differing trajectories for all ten classes of icebergs. The general pattern of iceberg drift between the four seasons is quite similar, and several features of an iceberg's trajectory after release into the Norwegian–Greenland basin from the western margin of the Eurasian Ice Sheet stand out. Firstly, icebergs of all class sizes move out into the Norwegian–Greenland basin in accordance with the westward currents and wind forcing applied to them. When the icebergs reach the convergence zone the wind forcing is in opposing directions and so the icebergs travel south with the ocean current, balanced by the winds either side. Class 1, being the smallest icebergs, are the first to melt in this journey southwards. The second main feature seen in all classes of icebergs is their tendency to cluster in this convergence zone, and so the majority of the icebergs' passage southwards is in quite a narrow band, about 100–150 km wide, in the Norwegian–Greenland basin. Within this band there is spread around the mean line of southwards travel, which is greatest in June (Fig. 8a, b), at around 400 km compared to 100 km in September (Fig. 9a,b). Another feature of the icebergs' tracks in the Norwegian–Greenland basin is the excursions made by all classes of icebergs across the Norwegian–Greenland Sea in response to the changing relative strengths of wind stress and therefore ocean currents. The exaggerated loop to the north of the basin is located where the westward branch of the Norwegian current intensifies, and weakens, with the associated wind stress. The different location of the loop between each iceberg class, with increasing size of icebergs resulting in an increase in offset to the north of about 10–20 km, illustrates the impact of the Coriolis force on an iceberg's trajectory. The Coriolis force is also evident in the icebergs transit southwards as the larger classes of icebergs flow to the right of the smaller classes, however, the impact of the Coriolis force decreases in the lower latitudes, and therefore the deflection is smaller, less than 10 km. A further characteristic of iceberg tracks in the Norwegian–Greenland basin is the secondary 'kink' in the icebergs tracks to the east of Iceland, resulting partly from changing ocean current strength and partly from a strengthening in the northward wind component from the North Atlantic.

As the icebergs cross the Faeroes–Iceland ridge another important feature is revealed in the trajectories. For icebergs of class 5 and above in the winter months (December and March) and for classes 8 and above in the summer months (June and September) a secondary cluster region develops. However, for the smaller class of icebergs this feature is absent as the icebergs melt too quickly. The icebergs travel south with the ocean currents out of the Norwegian and Greenland basin and then are turned around with both the ocean currents and wind forcing acting to reverse their direction. The result is that to the south-east of Iceland icebergs are concentrated as they get caught by the glacial sub-polar gyre. The position where the icebergs are turned round is partly determined by the iceberg size, and partly depends on the date of arrival at the Faeroes–Iceland ridge, due to subtle changes in the strength and structure of the sub-polar gyre and wind stress throughout the year. Once entrained in this dominant current they are taken westwards towards the south coast of Greenland. For all classes of icebergs, once they are entrained by this current they remain in it until they melt out.

The iceberg lifespan in this ocean current is strongly determined by the wind, through wave erosion, and the ocean sea surface temperature (Bigg et al., 1997). Therefore the date at which the icebergs enter the current is important as these variables change significantly through the year (Figs. 4 and 6). The summer release months have noticeably shorter tracks, as the warmer SSTs extend northwards. However, it is important to remember that the icebergs take time to travel through the Norwegian–Greenland basin, and it is the date of

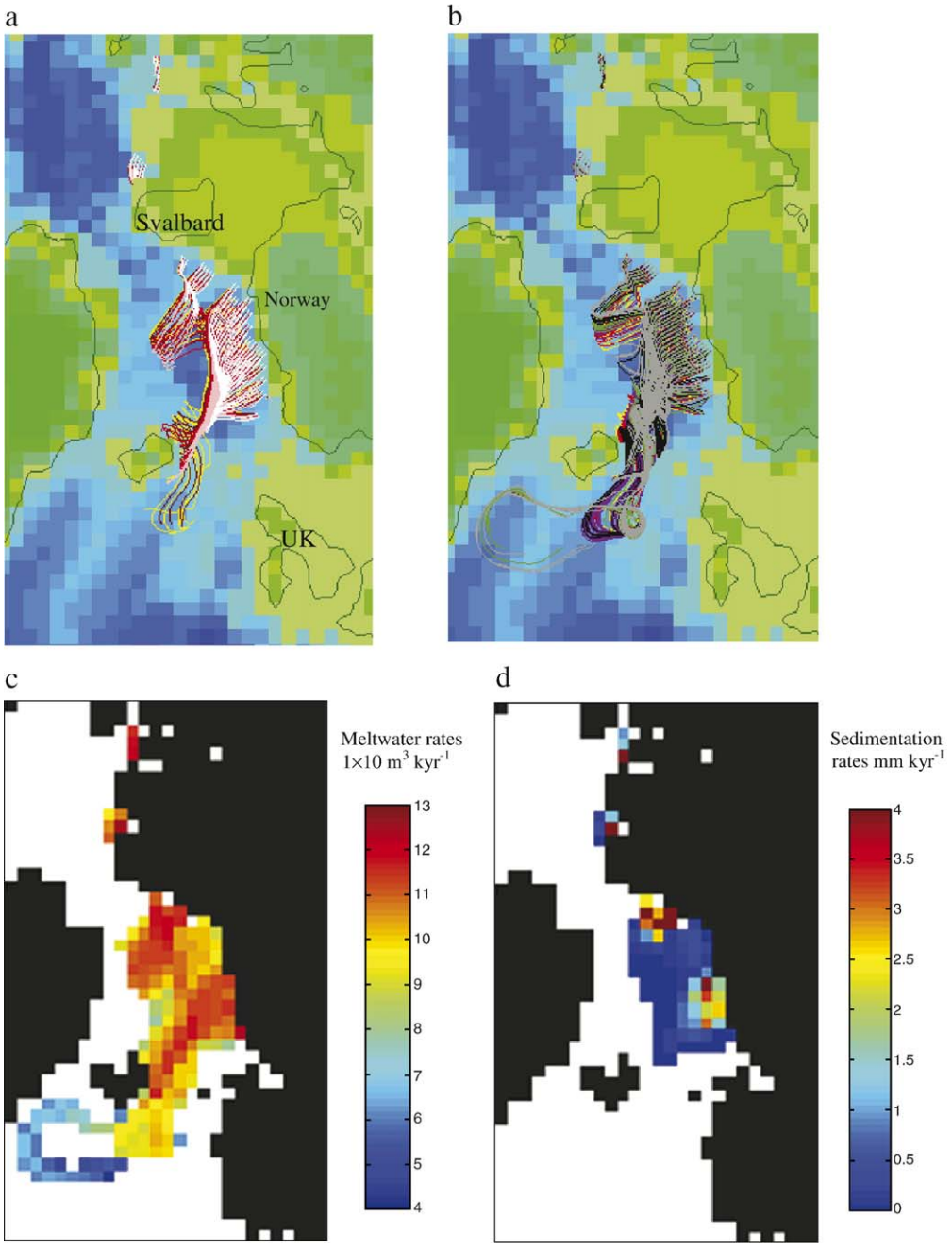

Fig. 7. (a,b) Iceberg trajectories after their release from the Eurasian Ice Sheet margin in April. The key for the iceberg tracks are: class 1 white; class 2 pink; class 3 orange; class 4 brown; class 5 yellow (a: Classes 1–5); class 6 red; class 7 purple; class 8 green; class 9 black; class 10 grey (b: Classes 6–10). The height of the topography is shown, with deeper blues corresponding to deeper ocean basins through to darker greens for higher land. (c) The meltwater rate for each 100 km^2 grid cell produced by the melting of all classes of icebergs released in March. (d) The sedimentation rates for each 100 km^2 grid cell produced by the basal melting of all classes of icebergs released in March.

arrival at the Iceland–Faeroes gateway that determines the iceberg's fate in the North Atlantic. In the region south of Iceland the winds are strongest and the SST warmest in September. Furthermore, as the structure of the glacial sub-polar gyre varies seasonally too, the degree to which the icebergs travel south into warmer water determines the length of survival of icebergs in this region of the North Atlantic.

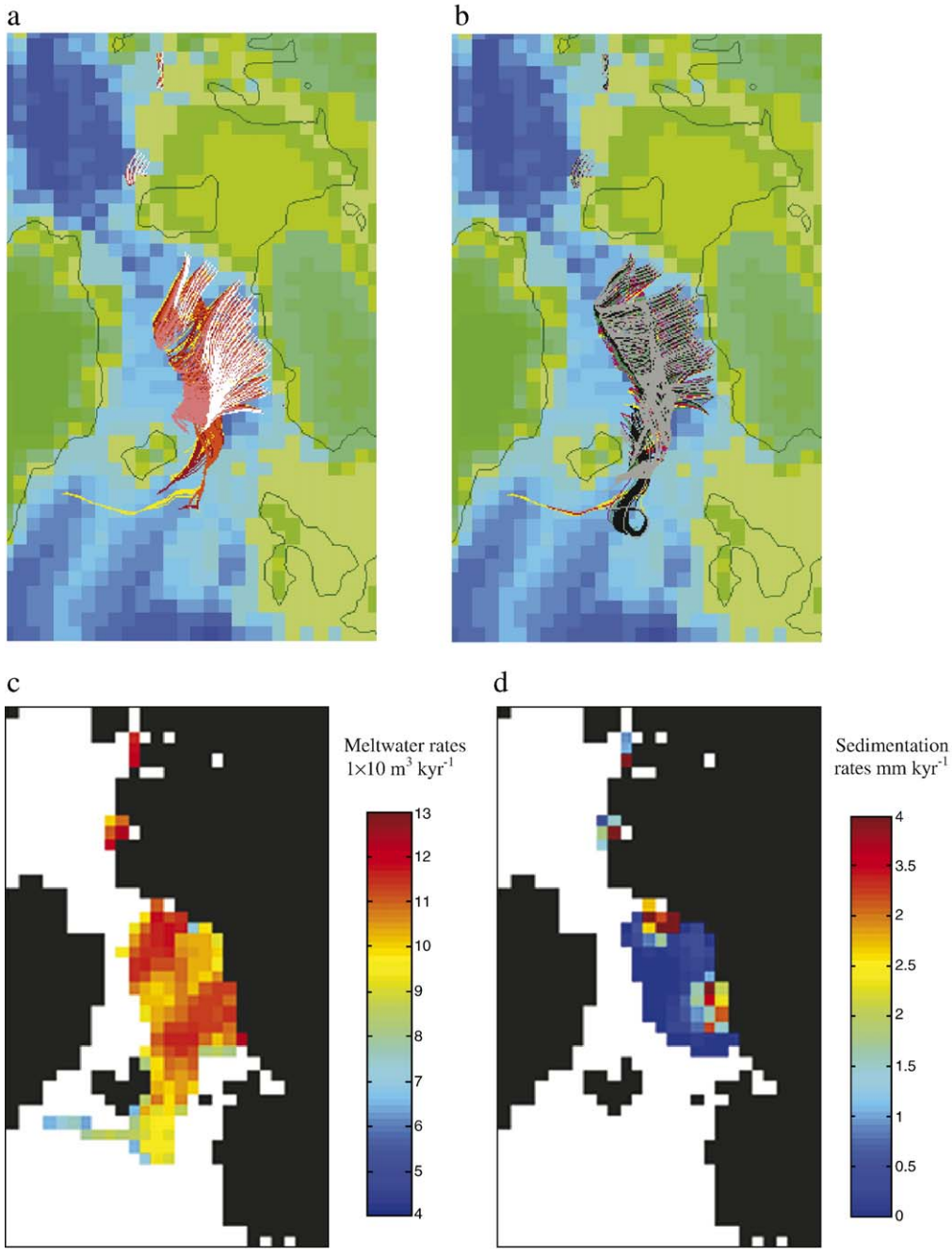

Fig. 8. (a, b) Iceberg trajectories after their release from the Eurasian Ice Sheet margin in June. The same key as for Fig. 7a and b, respectively. (c) The meltwater rate produced by the melting of all classes of icebergs released in June. The same key as for Fig. 7c. (d) The sedimentation rates produced by the basal melting of all classes of icebergs released in June. The same key as for Fig. 7d.

Finally, icebergs released from the northern margin of the Eurasian Ice Sheet into the Arctic Ocean are trapped against the coast by both the ocean currents and winds. The model therefore indicates that the deep scour marks found in the Arctic Ocean (Jakobsson, 1999) are unlikely to be from a Eurasian Ice Sheet source at the LGM.

3.2. Meltwater production

Figs. 7–9 and 10c show the meltwater pattern summarised for all iceberg classes for each season. As with the iceberg trajectories several traits in the meltwater patterns stand out. Firstly, the ice stream

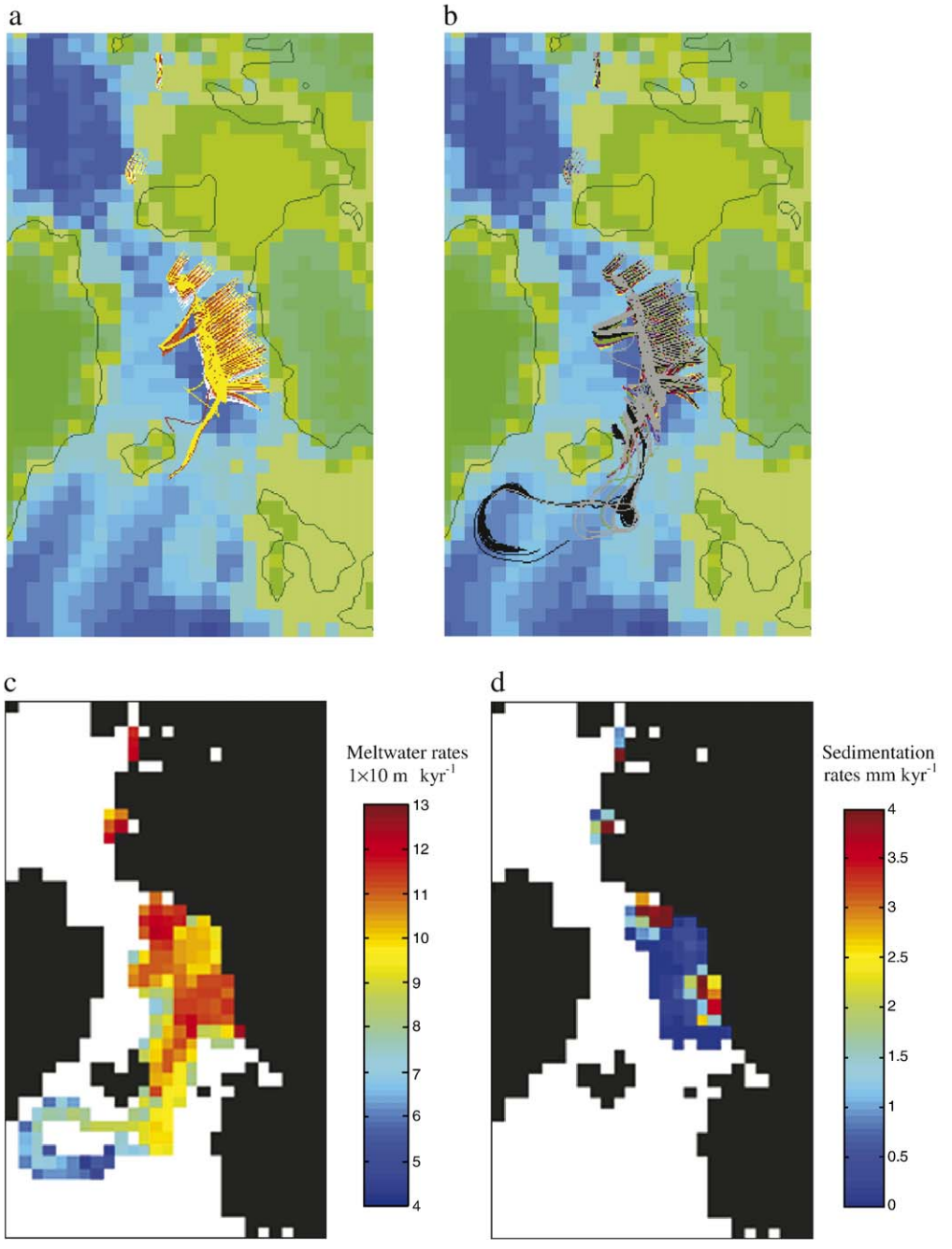

Fig. 9. (a, b) Iceberg trajectories after their release from the Eurasian Ice Sheet margin in September. The same key as for Fig. 7a and b, respectively. (c) The meltwater rate produced by the melting of all classes of icebergs released in September. The same key as for Fig. 7c. (d) The sedimentation rates produced by the basal melting of all classes of icebergs released in September. The same key as for Fig. 7d.

locations are clearly indicated by their associated production of meltwater plumes. These are seen for Storfjorden, the Bear Island Trough and the Norwegian channel ice streams on the western margin of the ice sheet, and at the St. Anna Trough and Franz–Victoria Trough on the northern margin. The icebergs released from the north melt out at the coastal margin. The degree to which the meltwater penetrates the northern region of the Norwegian–Greenland basin is controlled by the loop feature seen in the iceberg trajectories. The structure of the loop is also clearly shown in the meltwater patterns, with September and December

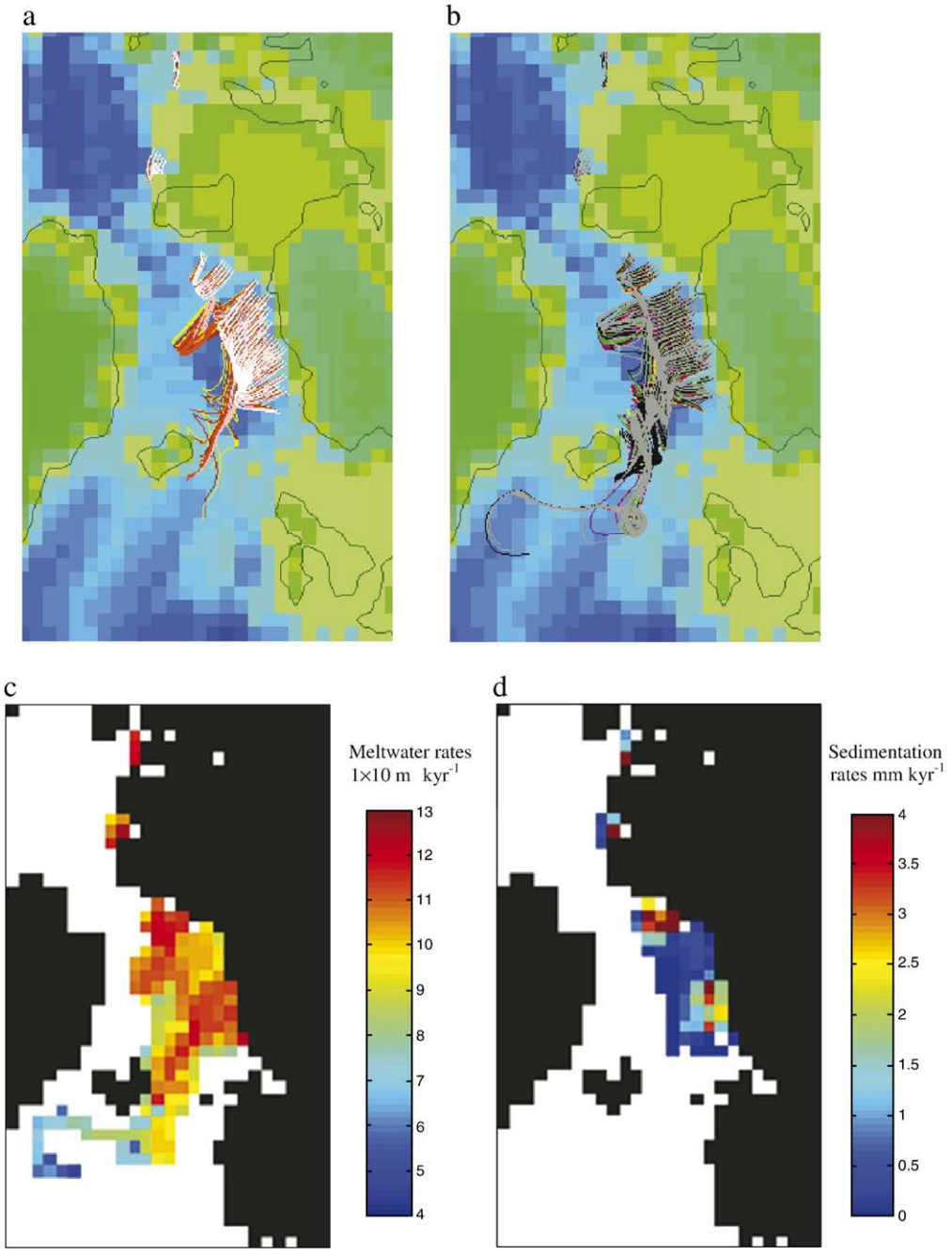

Fig. 10. (a, b) Iceberg trajectories after their release from the Eurasian Ice Sheet margin in December. The same key as for Fig. 7a and b, respectively. (c) The meltwater rate produced by the melting of all classes of icebergs released in December. The same key as for Fig. 7c. (d) The sedimentation rates produced by the basal melting of all classes of icebergs released in December. The same key as for Fig. 7d.

having thinner, 100–200 km wide, peaks compared to the broader, 300–500 km wide, peaks in March and June. The plume of meltwater from the southern Norway ice stream joins the meltwater produced by the concentration of icebergs travelling south in the convergence zone. The concentration of meltwater into these plumes may account for the localised relatively large excursions of $\delta^{18}O$ by 1–2‰, without an accompanying global signal. The modelled meltwater plume from the Barents Sea corresponds well with the location of the meltwater signal derived from $\delta^{18}O$ values by Sarnthein et al. (1995).

The second and perhaps most interesting feature in the meltwater pattern is the meltwater production associated with the two clustering zones. The first clustering of icebergs occurs as the icebergs travel southwards through the Norwegian–Greenland basin and are caught in the wind convergence zone. Although Figs. 7–9 and 10a,b show that the iceberg tracks oscillate across the convergence zone as the icebergs travel south, the band of relatively high melt remains quite stable at a distance of 400–500 km off the Norwegian coast. The characteristic of larger iceberg classes being deflected progressively to the right results in a distance-decay pattern in meltwater production to the right of the band of high meltwater production. A further characteristic of the meltwater pattern close to the western margin of the Eurasian Ice Sheet is the patch of relatively low meltwater production close to the north Norway coast. The icebergs in this region are quickly moved away from the coast by the surface ocean currents and wind forcing, so the time in which they can melt in a grid cell is decreased. The lower meltwater production near the coast compared to the offshore convergence zone in this region goes against previous conceptual thought about meltwater distribution from an ice sheet marine margin. The majority of iceberg melt, 70%, occurs in parts of the Norwegian–Greenland Seas.

The second clustering point southeast of Iceland though less intense is a good example of the importance of considering the impact of iceberg clustering in transporting relatively high meltwater inputs to regions distal from the ice sheet margin. Icebergs that are caught in this zone are held in relatively warmer water, 2–4 °C, from the North Atlantic. Therefore, the icebergs are not only being concentrated in their numbers, but are also melting quite rapidly at this point. It is this combination of dynamic and thermodynamic forcing that creates this area of relatively high meltwater input to the southeast of Iceland. The meltwater production in this region has a strong seasonal trend, with more meltwater released off the southeast of Iceland in the winter months ($>1\times10^{11}$ m^3 kyr^{-1}) compared to the summer (5×10^{8} m^3 kyr^{-1}) (Fig. 11). The decrease in meltwater production in this zone in the summer is due to the intrusion of warm water northwards melting icebergs out before they reach the southeast of Iceland.

The transportation of meltwater around the glacial sub-polar gyre derives from the relatively few icebergs that have not been melted in their excursion south. The tracks illustrate how the icebergs are transported back north to the relative cooler water, which allows them to survive their transport westwards. The East Greenland current, which is composed of very cold water, −1 to −2 °C, extends the icebergs survival as the iceberg travels southwards. However, once the icebergs travel far enough eastwards along the bottom part of the glacial sub-polar gyre they meet the relatively warmer water from the North Atlantic 2–4 °C (Fig. 6a–d) and therefore melt out. The impact of increased SST is clearly shown in the poor survival rates of icebergs in the glacial sub-polar gyre; icebergs that arrive in North Atlantic in the summer months melt out relatively early compared to those that arrive in the winter months. The effect of higher sea surface temperatures is two fold; directly it increases the temperature gradient between the iceberg and its surrounding water, while indirectly it increases the effectiveness of wave erosion, with both enhancing the magnitude of meltwater produced. The effect of sea-surface temperature on meltwater production is clearly seen in Fig. 12, where the total meltwater produced is totalled for all classes by month. There is a peak in meltwater production in August corresponding to sea surface temperature maxima in the southern Norwegian Sea. The importance of SST in controlling where melt occurs is further emphasised as the peak in melt of icebergs in the Norwegian Sea is in the summer months (Fig. 12).

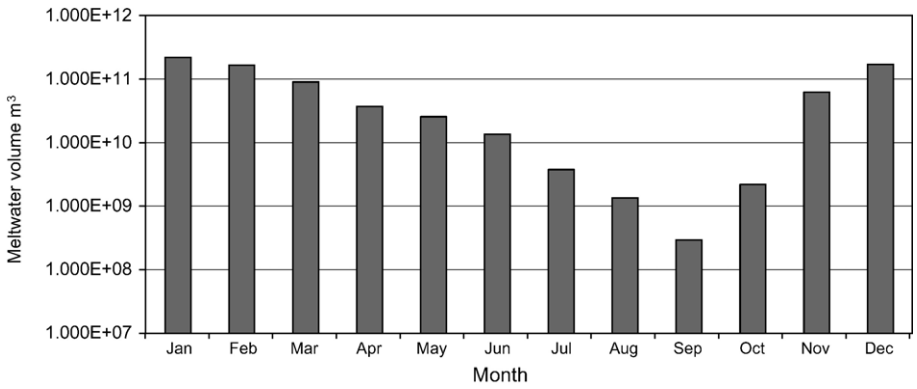

Fig. 11. The seasonal variation of meltwater release by icebergs of all classes off the Southeast of Iceland.

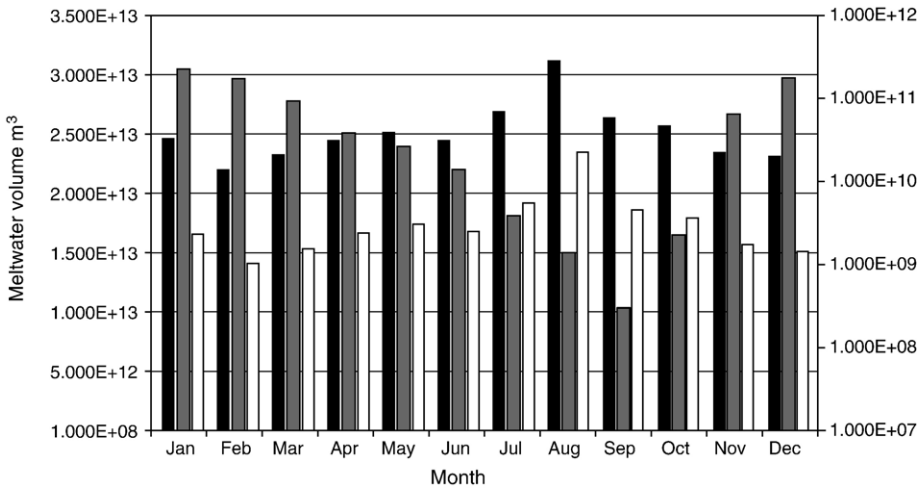

Fig. 12. The seasonal variability in total meltwater production for all classes of icebergs for all regions (black), compared to the meltwater release in the Norwegian–Greenland Sea (solid grey—left-hand axis), and meltwater release off Southeast Iceland (white—right-hand axis).

3.3. Sedimentation rates

Figs. 7–9 and 10d illustrate the sedimentation rates produced by all classes of icebergs for the four seasonal months. There are two striking features in the sedimentation rate patterns. Firstly, as with the meltwater production, the ice stream positions are easy to identify as they are characterised by enhanced sediment deposition. The sediment contribution from icebergs to the Bear Island fan is 48 mm kyr^{-1}, while to the south the sedimentation rate at the Norwegian Channel fan is around 24 mm kyr^{-1}. These figures therefore suggest that the iceberg contribution to total TMF sedimentation rate is ~3%. The sedimentation rates in these regions are the same order of magnitude as those estimated from sediment cores in the smaller Franz Victoria Trough of 4–21 cm kyr^{-1}(Knies et al., 2000).

The other defining feature of the sedimentation rate pattern is that it does not resemble the relatively high meltwater production at the two cluster sites described in the section above. The sedimentation pattern, if used as an indication of meltwater would suggest that iceberg meltwater production simply decreases with distance from the ice sheet margin. Furthermore, it would indicate that icebergs, and therefore meltwater production remained solely in the Norwegian–Greenland basin. The sedimentation rates fail to identify icebergs from the Eurasian Ice Sheet in the North Atlantic, even though there is a strong meltwater signal, especially off southeast Iceland, from these icebergs. As sediment is only carried in the basal layer in the model it is not surprising that it melts out early on in the iceberg's life. The drastically truncated sediment distribution compared to that of the meltwater argues strongly for sediment to be distributed more widely through last glacial icebergs issuing from the Eurasian Ice Sheet that penetrated into the Atlantic. There is little doubt that such southward penetration of Eurasian icebergs did occur (e.g. Gwiazda et al., 1996).

A mechanism by which sediment is transported englacially could account for IRD layers within the North Atlantic. Andrews et al. (1993) provide an appropriate method for incorporating sediment higher in the ice column by the freeze-on of super-cooled water. In this modelling experiment, for IRD from Scandinavia to reach the core sites at the Reykjanes Ridge (e.g. SU90-24; Elliot et al., 2001) sediment must be distributed throughout the iceberg (up to 200 m).

4. Conclusions

An ice sheet model was used to calculate the spatial locations and volumes of icebergs released from the Eurasian Ice Sheet at the LGM. These icebergs were input to a dynamic and thermodynamic iceberg model to determine the distribution of iceberg positions, meltwaters and sediments across the Greenland–Iceland–Norwegian seas. The iceberg model was forced with LGM atmospheric and ocean conditions derived from an atmospheric GCM (Dong and Valdes, 1998) and an ocean GCM (Wadley et al., 2002), respectively. From analysis of the model results the following conclusions were made:

- After release from the parent ice mass, icebergs were found to collect in atmospheric and/or ocean

convergence zones. Two main collection zones were identified; one in the Norwegian–Greenland basin, and one to the southeast of Iceland.

- The meltwater distribution produced by icebergs reflects their complex trajectories. In the Greenland–Iceland–Norwegian seas Eurasian icebergs were responsible for relatively high volumes of meltwater in zones often distal (greater than 600 km) to the ice-sheet margin.
- The glacial sub-polar gyre has a strong influence on an iceberg position once it exits the Norwegian–Greenland basin, and therefore melt in the North Atlantic from the Eurasian Ice Sheet tends to follow the surface ocean current of this gyre system.
- Modelled sedimentation rates from icebergs are not found to be a good indicator of meltwater input from the Eurasian Ice Sheet if sediment is assumed to be confined to a basal layer.
- The presence of Ice Rafted Debris (IRD) in marine sediment does provide an indication of iceberg melt; however, from this modelling investigation the absence of IRD should not necessarily be used to indicate the absence of former iceberg melt in high latitude oceans.

Acknowledgements

Funding for this project was provided by UK NERC Ph.D. studentship NER/S/A/2000/03193 to RD. We acknowledge John Andrews and an anonymous reviewer for their helpful comments which improved the paper.

References

Alley, R.B., 1998. Icing the North Atlantic. Nature 392, 335–337.

Andrews, J.T., Tedesco, K., Jennings, A.E., 1993. Heinrich events: chronology and processes, east-central Laurentide Ice Sheet and NW Labrador Sea. In: Peltier, W.R. (Ed.), Ice in the Climate System. Springer-Verlag, Berlin, pp. 167–186.

Bard, E., Rostek, F., Turon, J.-L., Gendreau, S., 2000. Hydrological impact of Heinrich events in the subtropical northeast Atlantic. Science 289, 1321–1324.

Bauch, H.A., Erlenkeuser, H., Spielhagen, R.F., Struck, U., Matthiessen, J., Thiede, J., Heinemeier, J., 2001. A multiproxy reconstruction of the evolution of deep and surface waters in the subarctic Nordic seas over the last 30,000 years. Quaternary Science Reviews 20, 659–678.

Bigg, G.R., Wadley, M.R., Stevens, D.P., Johnson, J.A., 1997. Modelling the dynamics and thermodynamics of icebergs. Cold Regions Science and Technology 26, 113–135.

Bond, G., Broecker, W.S., Johnsen, S., McManus, J., Labeyrie, L., Jouzel, J., Bonani, G., 1993. Correlations between climate records from the North Atlantic sediments and Greenland ice. Nature 365, 143–147.

Clarke, G.K.C., La Prairie, D.I., 2001. Modelling iceberg drift and ice-rafted sedimentation. In: Straughan, B., Greve, R., Ehrentraut, H., Wang, Y. (Eds.), Continuum Mechanics and Applications in Geophysics and the Environment. Springer-Verlag, Berlin.

Dong, B., Valdes, P.J., 1998. Simulations of the Last Glacial Maximum climates using a general circulation model: prescribed versus computed sea surface temperatures. Climate Dynamics 14, 571–591.

Dowdeswell, J.A., Murray, O., 1990. Modelling rates of sedimentation from icebergs. In: Dowdeswell, J.A., Scourse, J.D. (Eds.), Glacimarine Environments: Processes and Sediments. Geological Society Special Publication, vol. 53, pp. 121–137.

Dowdeswell, J.A., Whittington, R.J., Hodgkins, R., 1992. The sizes, frequencies and freeboards of East Greenland icebergs observed using ship radar and sextant. Journal of Geophysical Research 97, 3515–3528.

Dowdeswell, J.A., Maslin, M.A., Andrews, J.T., McCave, I.N., 1995. Iceberg production, debris rafting and extent and thickness of Heinrich layers (H-1, H-2) in North Atlantic sediments. Geology 23, 301–304.

Duplessy, J.-C., Labeyrie, L., Waelbroeck, C., 2002. Constraints on the ocean oxygen isotopic enrichment between the Last Glacial Maximum and the Holocene: palaeoceanographic implications. Quaternary Science Reviews 21, 315–350.

Elliot, M., Labeyrie, L., Dokken, T., Manthé, S., 2001. Coherent patterns of ice-rafting debris deposits in the Nordic regions during the last glacial (10–60 ka). Earth and Planetary Science Letters 194, 151–163.

Gladstone, R., Bigg, G.R., Nicholls, K., 2001. Icebergs and fresh water fluxes in the Southern Ocean. Journal of Geophysical Research 106, 19903–19915.

Grousset, F.E., Labeyrie, L., Sinko, J.A., Cremer, M., Bond, G., Duprat, J., Cortijo, E., Huon, S., 1993. Patterns of ice-rafted detritus in the glacial North Atlantic (40–55°N). Paleoceanography 8, 175–192.

Grousset, F.E., Cortijo, E., Huon, S., Hervé, L., Richter, T., Burdloff, D., Duprat, J., Weber, O., 2001. Zooming in on Heinrich layers. Paleoceanography 16, 240–259.

Gustajitis, K.A., Buckley, T.J., 1978. A seasonal iceberg density distribution along the Labrador coast. In: Muggeridge, D.B. (Ed.), Fourth International Conference on Port and Ocean Engineering under Arctic Conditions. Memorial University of New Foundland, St. John's, New Foundland, pp. 972–983.

Gwiazda, Hemming, S.R., Broecker, W.S., 1996. Provenance of icebergs during Heinrich event 3 and the contrast to their sources during other Heinrich episodes. Paleoceanography 11 (4), 371–378.

Hebbeln, D., Henrich, R., Baumann, K.-H., 1998. Paleoceanography of the last interglacial/glacial cycle in the polar North Atlantic. Quaternary Science Reviews 17, 125–153.

Heinrich, H., 1988. Origin and consequences of cyclic ice rafting in the northeast Atlantic Ocean during the past 130,000 years. Quaternary Research 29, 143–152.

Jakobsson, M., 1999. First high resolution chirp sonar profiles from the central Arctic Ocean reveal erosion of Lomonosov Ridge sediments. Marine Geology 158, 111–123.

Knies, J., Nowaczyk, N., Muller, C., Vogt, C., Stein, R., 2000. A multiproxy approach to reconstruct the environmental changes along the Eurasian continental margin over the last 150 000 years. Marine Geology 163, 317–344.

Koç, N., Jansen, E., Haflidason, H., 1993. Paleoceanographic reconstructions of surface ocean conditions in the Greenland,

Iceland and Norwegian Seas through the last 14 ka based on diatoms. Quaternary Science Reviews 12, 115–140.

MacAyeal, D.R., 1993. Binge–purge oscillations of the Laurentide Ice Sheet as a cause of the North Atlantic's Heinrich events. Paleoceanography 8, 775–784.

Matsumoto, K., 1996. An iceberg drift and decay model to compute the ice-rafted debris and iceberg meltwater flux: application to the interglacial North Atlantic. Paleoceanography 11, 729–742.

Matsumoto, K., 1997. Modeled glacial North Atlantic ice-rafted debris pattern and its sensitivity to various boundary conditions. Paleoceanography 12, 271–280.

NGDC, 1986. ETOPO-5 bathymetery/topography data. Data Announcement 88-MGG-02, National Oceanic and Atmospheric Administration, US Dep. Commer., Boulder, Colorado.

Prins, M.A., Bouwer, L.M., Beets, C.J., Troelstra, S.R., Weltje, G.J., Kruk, R.W., Kuijpers, A., Vroon, P.Z., 2002. Ocean circulation and iceberg discharge in the glacial North Atlantic: inferences from unmixing of sediment size distributions. Geology 30 (6), 555–558.

Rahmstorf, S., 2002. Ocean circulation and climate during the past 120,000 years. Nature 419, 207–214.

Raymo, M.E., Ruddiman, W.F., Shackleton, N.J., Oppo, D.W., 1990. Evolution of Atlantic–Pacific $\delta^{13}C$ gradients over the last 2.5 m.y. Earth and Planetary Science letters 97, 353–368.

Sarnthein, M., Jansen, E., Weinelt, M., Arnold, M., Duplessy, J.-C., Erlenkeuser, H., Flatøy, A., Johannessen, G., Johannessen, T., Jung, S., Koc, N., Labeyrie, L., Maslin, M., Pflaumann, U., Schulz, H., 1995. Variations in Atlantic surface ocean paleoceanography, 50°–80°N: a time-slice record of the last 30,000 years. Paleoceanography 10 (6), 1063–1094.

Siegert, M.J., Dowdeswell, J.A., Melles, M., 1999. Late Weichselian glaciation of the Eurasian High Arctic. Quaternary Research 52, 273–285.

Siegert, M.J., Dowdeswell, J.A., Elverhøi, A., Svendsen, J.-I., 2002. The Eurasian Arctic during the last Ice Age. American Scientist 90, 32–39.

Svendsen, J.I., Astakov, V.I., Bolshiyanov, D.Yu, Demidov, I., Dowdeswell, J.A., Gataullin, V., Hjort, Ch., Hubberten, H.W., Larsen, E., Mangerud, J., Melles, M., Möller, P., Saarnisto, M., Siegert, M.J., 1999. Maximum extent of the Eurasian Ice Sheets in the Barents and Kara Sea region during the Weichselian. Boreas 28, 234–242.

Wadley, M.R., Bigg, G.R., Rohling, E.J., Payne, A.J., 2002. On modelling present day and Last Glacial Maximum oceanic $\delta^{18}O$ distributions. Global and Planetary Change 32, 89–109.

Weeks, W.F., Mellor, M., 1978. Some elements of icebergs technology. In: Husseiny, A.A. (Ed.), Proceedings of the First Conference on Iceberg Utilization for Freshwater Production. Iowa State University, pp. 45–98.